Author Manuscript

Author Manuscript

Author Manuscript

Author Manuscript

HHS Public Access

Author manuscript

Colloids Surf B Biointerfaces. Author manuscript; available in PMC 2019 June 01.

Published in final edited form as:

Colloids Surf B Biointerfaces. 2018 June 01; 166: 98–107. doi:10.1016/j.colsurfb.2018.03.011.

Adsorption and decontamination of α-synuclein from medically and environmentally-relevant surfaces

Hanh T.M. Phan[1,5], **Jason C. Bartz**[2], **Jacob Ayers**[3], **Benoit I. Giasson**[3], **Mathias Schubert**[4,5], **Keith B. Rodenhausen**[4,5,6], **Negin Kananizadeh**[1,5], **Yusong Li**[1], and **Shannon L. Bartelt-Hunt**[1,5,*]

[1]Department of Civil Engineering, University of Nebraska-Lincoln

[2]Department of Medical Microbiology and Immunology, Creighton University

[3]Department of Neuroscience, University of Florida

[4]Department of Electrical and Computer Engineering, University of Nebraska-Lincoln

[5]Center for Nanohybrid Functional Materials, University of Nebraska-Lincoln

[6]Biolin Scientific, Inc., Paramus, New Jersey

Abstract

The assembly and accumulation of α-synuclein fibrils are implicated in the development of several neurodegenerative disorders including multiple system atrophy and Parkinson's disease. Pre-existing α-synuclein fibrils can recruit and convert soluble non-fibrillar α-synuclein to the fibrillar form similar to what is observed in prion diseases. This raises concerns regarding attachment of fibrillary α-synuclein to medical instruments and subsequent exposure of patients to α-synuclein similar to what has been observed in iatrogenic transmission of prions. Here, we evaluated adsorption and desorption of α-synuclein to two surfaces: stainless steel and a gold surface coated with a 11-Amino-1-undecanethiol hydrochloride self-assembled-monolayer (SAM) using *in-situ* combinatorial quartz crystal microbalance with dissipation and spectroscopic ellipsometry. α-Synuclein was found to attach to both surfaces, however, increased α-synuclein adsorption was observed onto the positively charged SAM surface compared to the stainless steel surface. Dynamic light scattering data showed that larger α-synuclein fibrils were preferentially attached to the stainless steel surface when compared with the distributions in the original α-synuclein solution and on the SAM surface. We determined that after attachment, introduction of a 1N NaOH solution could completely remove α-synuclein adsorbed on the stainless steel surface while α-synuclein was retained on the SAM surface. Our results indicate α-synuclein can bind to multiple surface types and that decontamination is surface-dependent.

*Corresponding Author: sbartelt2@unl.edu (SB), Postal address: 1110 S. 67th St., Omaha, Nebraska 68182-0178.

Publisher's Disclaimer: This is a PDF file of an unedited manuscript that has been accepted for publication. As a service to our customers we are providing this early version of the manuscript. The manuscript will undergo copyediting, typesetting, and review of the resulting proof before it is published in its final citable form. Please note that during the production process errors may be discovered which could affect the content, and all legal disclaimers that apply to the journal pertain.

AUTHOR CONTRIBUTIONS

HTMP designed experiments, performed experiments, analyzed data and wrote the manuscript; SLB and JCB designed experiments, analyzed data and wrote the manuscript; JA and BIG supplied unique materials (α-synuclein protein) and wrote the manuscript; MS, KBR, NK and YL analyzed data and wrote the manuscript. All authors have read and approved of the manuscript.

Author Manuscript Author Manuscript Author Manuscript Author Manuscript

Graphical abstract

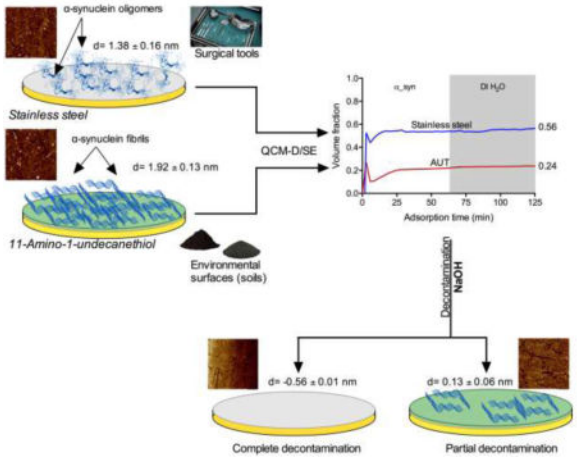

Keywords

α-Synuclein; stainless steel; adsorption; decontamination; QCM-D; Spectroscopic Ellipsometry; protein conformation; protein orientation

Introduction

Synucleinopathies are a group of neurodegenerative diseases that include Parkinson's disease (PD), dementia with Lewy bodies, and multiple system atrophy (MSA)[1-4]. These diseases are characterized by the accumulation of a fibrillar form of α-synuclein (α-syn) in the central nervous system (CNS)[3]. Mutations in the gene that encode α-syn (SNCA) correspond with familial forms of PD, suggesting a causal role of α-syn[3, 5, 6]. Nevertheless, the relationship between α-syn accumulation and disease development is still not completely understood.

Fibrillar α-syn shares many features with prions[7-9], the infectious protein that is the causative agent for prion diseases. Prion diseases or transmissible spongiform encephalopathies (TSEs), are a group of neurodegenerative diseases occurring in animals such as Scrapie (sheep and goat), Chronic Wasting Disease (CWD) (deer, moose and elk), Bovine Spongiform Encephalopathy (BSE) (cattle), or in human such as Creutzfeldt-Jakob Disease (CJD)[10]. Fibrillar α-syn directs the conversion of soluble forms of α-syn to fibrillar forms, similar to prions[8], where the infectious form of the prion protein (PrP^{Sc}) can intriguingly initiate and replicate misfolding of PrP^{C}, the normal form of the protein. Similarly, conversion of soluble α-syn can explain the formation and spread of fibrillar α-syn between cells in culture[7, 8, 11]. Injection of fibrillar α-syn into the central or peripheral nervous system results in the spread of fibrillar α-syn throughout the CNS along neuroanatomical connections similar to what is observed in prion diseases[5, 7-9]. This experimental result is consistent with spread of pathology along neuroanatomical tracks in the CNS of patients with PD[8]. Interestingly, intramuscular[12], intraperitoneal[13] or

Author Manuscript Author Manuscript Author Manuscript Author Manuscript

intravenous[14] injection of fibrillar α-syn can result in α-syn inclusion pathology in the CNS. The mechanism by which neuroinvasion of fibrillar α-syn occurs is likely complex[8].

Iatrogenic transmission can occur from prion-contaminated surfaces[15-18]. Human prion diseases are not robustly contagious, however, they can be transmitted in medical settings from contaminated surgical instruments[17-20]. Consistent with this observation, stainless steel can bind prions[16, 21, 22] and prions survive standard hospital sterilization procedures[16, 18, 21-28]. The mechanism by which prions bind to surfaces and whether desorption from the surface is required to establish infection are not known[16]. The long asymptomatic phase of prion disease, poor preclinical diagnostic tests, and the relative resistance of prions to standard decontamination treatments[25-28] exacerbate the risk of prion transmission. So far, there is no evidence of epidemiological transmission of α-syn. The potential risk of α-syn transmission was experimentally demonstrated where MSA prion contaminated stainless steel wires induced robust α-syn propagation in transgenic mice expressing mutated human α-syn[29] using similar transmission paradigms previously used for prions[22]. Despite the emerging concerns of iatrogenic transmission of α-syn, there is limited knowledge about fibrillar α-syn adsorption or desorption to surfaces.

Information on the binding and release of fibrillar α-syn to and from surfaces is limited[21]. Previous studies have investigated the interaction of soluble α-syn to positively charged poly(allylamine hydrochloride) coated or uncoated gold nanoparticles and found that α-syn can bind to these particles via multilayer adsorption and electrostatic interactions[30, 31]. α-Syn in human brain homogenate was determined to bind to stainless steel and can be partially removed[21].

Prions can bind to environmental surfaces and remain infectious after years in the environment[27, 32-36]. Prions can adsorb to a wide range of soils and soil minerals and the adsorption is strongly irreversible which is resistant to most inactivation treatments for conventional pathogens[37, 38]. Since fibrillar α-syn and prions share many common traits, there is an interest in behavior of fibrillar α-syn after binding to environmental surfaces, although there is limited information regarding fibrillar α-syn adsorption to or desorption from environmental surfaces.

To further investigate the interaction of α-syn with environmentally- and medically-relevant surfaces, we used quartz crystal microbalance with dissipation (QCM-D) and spectroscopic ellipsometry (SE) allowing for real-time, in-situ monitoring of adsorbate thickness, mass, and porosity (i.e., surface conformation). QCM-D/SE can provide insight into protein interactions at solid/liquid interfaces including structural arrangements[39, 40], cooperative adsorption, cross-linking, adsorption kinetics, and protein aggregation on the nanoscale[41]. Decontamination of α-syn from contaminated surfaces using 1N sodium hydroxide solution (NaOH) was also quantitatively measured with QCM-D and SE. The objective of this study was to investigate the dynamic adsorption of α-syn onto surfaces and the effectiveness of a proposed decontaminant. In this study, α-syn in the form of amyloid fibrils was used to deposit on stainless steel and 11-Amino-1-undecanthiol hydrochloride (AUT) self-assembled-monolayer (SAM) surface. Stainless steel was used as medically relevant surface and AUT was used as representative for environmentally relevant surfaces, as the AUT SAM

Author Manuscript Author Manuscript Author Manuscript Author Manuscript

surface was demonstrated in a prior work by the authors to have the greatest adsorption capacity for proteins compared to neutral or negatively charged SAM surfaces[41].

α-Syn is a 140 amino acid residue protein with three domains, including an N-terminus domain, a central domain (NAC), and a C-terminus domain[30, 42, 43]. The positively charged N-terminal domain (residues 1–60) contains four series of 11-AA repeats with a highly conserved KTKEGV hexameric motif on each repeat[30, 44]. The core region NAC (residues 61–95) is a hydrophobic and highly amyloidogenic central domain[45], which involved in fibril formation and aggregation[46] as it can form cross β-structures[47]. The C-terminal acidic tail (residues 96–140) includes 15 carboxylate groups[44] and forms a random coil structure in aqueous solution due to its low hydrophobicity and high net negative charge[42, 43]. In addition, α-syn with pI of 4.7 has negative surface charge in DI H_2O (pH ~ 5.6) and can fold into various conformations depending on the environment and conditions[48, 49].

Materials and Methods

Recombinant α-syn expression, purification and amyloid fibril formation

The pRK172 bacterial expression vector containing the cDNA encoding wild-type, full-length human α-syn was previously described[50, 51]. The plasmid was transformed into BL21 (DE3)/RIL *Escherichia coli* (*E. coli*; Agilent Technologies) and recombinant α-syn was purified from *E. coli* by size exclusion chromatography and subsequent anion exchange as previously described[50, 51]. Protein concentrations were determined by bicinchoninic acid assay using bovine serum albumin as the protein standard. Recombinant α-syn (5 mg/mL in sterile phosphate buffered saline was incubated at 37°C with constant shaking at 1050 rpm (Thermomixer R, Eppendorf) for 7 days that results in polymerization in amyloid fibril[50, 51]. Fibril formation was monitored by K114 ((trans,trans)-1-bromo-2,5-bis-(4-hydroxy)styrylbenzene) fluorometry as previously described[52]. α-syn fibril solution was diluted to 10 using DI H_2O and used in this study (unless otherwise specified).

BSA solution—The bovine serum albumin (BSA) stock solution was made by dissolving BSA powder (Fisher Scientific) in DI H_2O to a final concentration of 10 μg/mL. BSA is a globular protein with the approximate shape of a prolate spheroid in aqueous solution[53] and used as a standard protein solution with pI ~ 4.7.

Stainless steel surface—Quartz crystal sensors coated with a 50 nm 316-graded stainless steel layer (Biolin Scientific) were used as stainless steel substrates. New sensors were rinsed with 1% Hellmanex II and dried with nitrogen gas before an experiment. The stainless steel surface has pI ~ 3–4[54] and carries a negative surface charge in DI H_2O.

AUT surface—11-Amino-1-undecanthiol hydrochloride (AUT, > 90%, Dojindo), with a hydrophilic amine ($–NH_2$) terminal functional group, was used as the self-assembled-monolayer (SAM). At the neutral pH condition (pH 6.7), AUT is positively charged. The AUT SAM is well characterized and used extensively as model surfaces[55, 56]. n-Alkanethiols attach to Au surfaces by chemisorption at a thiol group to form close-packed SAM, leaving the functional groups other end ($–NH_2$) available to bind proteins[57]. To prepare the AUT surface, 2.0 mM AUT solution was prepared using filtered and degassed

Author Manuscript Author Manuscript Author Manuscript Author Manuscript

200-proof ethanol (Fisher Scientific). Quartz crystal sensors coated with a 100 nm Au layer (Biolin Scientific) were used as substrates. The Au-coated sensors were first rinsed with acetone (Fisher Scientific) followed by 200-proof ethanol. The AUT was formed by immersing the sensor in 20 mL of 2.0 mM AUT solution in an amber bottle covered by Ar gas stream for at least 60 mins at room temperature. The prepared AUT-coated Au sensors were then rinsed with 200 proof ethanol to ensure the removal of physically-absorbed thiol molecules. The AUT surfaces were dried under nitrogen gas.

Ex-situ ellipsometry

Ex-situ ellipsometry measurements were done under ambient air to characterize the stainless steel and AUT surfaces. *Ex-situ* ellipsometry measurements were performed as described previously[41]. Briefly, *ex-situ* ellipsometry measurements were made using a RC2-DI Ellipsometer (J.A. Woollam Co., Inc.) to evaluate changes in organic adsorbate thickness after protein/molecules adsorption/desorption on surfaces. *Ex-situ* ellipsometry measurements were made at room temperature in the spectral range of 370-1690 nm and at multiple angles of incidence with respect to the substrate normal from 45° to 75° in 10° increments. We used a two-layer substrate-organic layer optical model. A Cauchy layer modeled the totality of organic adsorbate, where the extinction coefficient k is necessarily zero and where we assumed the index of refraction $n_o = 1.5$. Thus, the Cauchy layer represented the combined AUT and α-syn layer on the Au surface, and the α-syn (or BSA) layer on the stainless steel surface. The optical constants of the stainless steel and Au surfaces were determined from measurements taken before α-syn adsorption, while the Cauchy layer had a thickness of zero. The Cauchy layer thickness was then allowed to vary by the optical model as model-calculated data and the experimental data taken after adsorption were best-matched by the WVASE software package (J.A.Woollam Co., Inc.), and the Cauchy thickness was recorded.

In-situ combinatorial QCM-D/SE

α-Syn adsorption to stainless steel and AUT-coated Au surfaces was monitored in real-time using *in-situ* combinatorial QCM-D/SE. Details about data acquisition and comparison between QCM-D and SE are described in a prior study[58]. Briefly, for a solvated organic adsorbate layer, such as proteins, QCM-D is sensitive to the mass of both attached adsorbate and ambient liquid that is coupled to the adsorbate. For porous, transparent adsorbate layers with thickness that is very small compared to the wavelength of probing light (i.e., on the order of 10 nm or less), SE is not sensitive to ambient liquid within the adsorbate layer. Thus, the adsorbate volumetric porosity ($f_{o,V}$) may be determined if the SE-determined thickness (d_{SE}) and the QCM-D-determined thickness (d_{QCMD}) are known. For the special case where the adsorbate and liquid densities are assumed equivalent (for simplicity, we assumed proteins and DI H_2O densities equal 1 kg/m^3), $f_{o,V}$ is the ratio of d_{SE} to d_{QCMD} [58, 59].

The combinatorial QCM-D/SE instrumentation consists of an M-2000-V SE (J. A. Woollam Co., Inc.), which measures 512 wavelengths in the visible and near-infrared spectrum simultaneously (370 – 1000 nm), and a mounted Explorer QCM-D (Biolin Scientific). The optical model for *in-situ* measurements was a two-layer, substrate (stainless steel or Au) –

Author Manuscript Author Manuscript Author Manuscript Author Manuscript

adsorbate (α-syn, BSA, or AUT-bound α-syn), under ambient DI H_2O solution. Similarly, the adsorbate layer was modeled by a Cauchy layer assuming $n_o = 1.5$.

Prior to the *in-situ* QCM-D/SE measurement of α-syn (or BSA) adsorption onto stainless steel and AUT surfaces, three *ex-situ* SE measurements (including ambient air without liquid cell, ambient air with liquid cell, and ambient DI H_2O with liquid cell) at multiple angles of incidence were taken to develop the optical model for each of the surfaces. Starting values were taken from the two-layer optical model described above. Details of the three ex-*situ* QCM-D/SE measurements were described in Supporting Information.

Thickness, mass, and porosity changes in SE and QCM-D induced by α-syn attachment were monitored continuously, and data acquisition was performed using the CompleteEASE (J.A. Woollam Co., Inc) and QSoft (Biolin Scientific) software packages for SE and QCM-D, respectively. Triplicate QCM-D/SE measurements for each type of surface were performed.

QCM-D data analysis

The Sauerbrey equation and the Voigt-Kelvin model were used to quantify adsorption of proteins on stainless steel and AUT surfaces, respectively. The Sauerbrey equation is used for rigid thin films while Voigt-Kelvin model is used for viscoelastic thin films. Details about the Sauerbrey equation and the Voigt-Kelvin model were presented in several papers[39, 59-61]. When normalized measured frequency shifts $\Delta f_n/n$ (n: overtone order) are independent of the overtone order, and if the dissipation shift ΔD_n is very small relative to $\Delta f_n/n$ (with a criterion: $\Delta D_n/(-\Delta f_n/n) < 5 \times 10^{-8}$ HZ^{-1} for a 5 MHz crystal), the film is assumed to be rigid. When the $\Delta f_n/n$ are spread between various orders and ΔD_n are significant with respect to $\Delta f_n/n$ (the above criterion is not met), the viscoelastic properties of the film need to be considered. For α-syn and BSA adsorption on stainless steel surfaces, QCM-D data demonstrated that the organic thin film was assumed to be rigid (Fig S1 and Fig S2) while α-syn adsorption on AUT surface was found to be viscoelastic (Fig S1). Therefore, QCM-D thickness was calculated using the Sauerbrey equation with the 3rd frequency overtone[58, 59] for α-syn and BSA adsorption on stainless steel surfaces and the Voigt-Kelvin model (with 3rd, 5th, and 7th overtones) was applied for the α-syn adsorption on the AUT surface.

QCM-D/SE data are statistically presented from triplicate experiments from which adsorbed thickness, volume fraction and corresponding standard error values were determined[62]. The α-syn adsorption/desorption rates over a specific period of time was calculated by dividing the areal mass of adsorbed α-syn by the adsorption/desorption time[63].

Decontamination/desorption experiments—α-Syn and BSA were removed from surfaces with 1N NaOH solution, which was diluted from purified 10N NaOH (Fisher Scientific). Immediately following QCM-D/SE measurements, the contaminated surfaces were submerged into the 1N NaOH solution for 1 hr at room temperature and then thoroughly rinsed with DI H_2O to remove NaOH and any desorbed α-syn molecules. NaOH/rinsed DI H_2O mixture was collected for DLS measurements. The sensor was dried with nitrogen gas and the thickness was measured immediately before and after the

Author Manuscript Author Manuscript Author Manuscript Author Manuscript

decontamination using *ex-situ* ellipsometry as described above. The sensor was then stored at −80°C for further AFM imaging described below.

Dynamic Light Scattering (DLS)—Size, size distribution, and zeta-potential of the protein solutions and effluents were measured using a Brookhaven Zeta PALS instrument. Samples for DLS measurements included the influent α-syn solution at 10 μg/mL, the influent BSA solution at 10 μg/mL, the effluent 1 (before NaOH) collected when the valve is switched from the α-syn phase to the first DI H_2O phase (at minute 60) in QCM-D/SE experiment, and the effluent 2 (after NaOH) was collected after the NaOH decontamination experiment. Each sample was loaded to a cuvette and five runs were performed. The data of 6 replicates were collected in number percentage of various particle sizes and weighted for each particle size. An average of weighted particle sizes were preformed.

Atomic Forced Microscopy (AFM)—A Dimension Icon with ScanAyst (Bruker, Santa Barbara, CA, USA) was used to image stainless steel and AUT surfaces before adsorption, after α-syn deposition, and after decontamination. A new stainless steel surface and AUT-coated Au sensor were prepared as described above before imaging. After the adsorption/desorption, the sensor was taken out from the QCM-D/SE liquid cell/NaOH solution, rinsed with DI H_2O and air dried before imaging. A mica sample was prepared by placing 1 mL of a 10 μg/mL concentration α-syn solution on a freshly cleaved mica plate (12.7 mm, Fisher Scientific) which was allowed to air dry for 1 hour in room temperature before imaging. AFM images were acquired in air using PeakForce Tapping technique. All images were captured with a resolution of 512 samples/line and a scan rate of 0.977 Hz.

Results

α-syn adsorption onto stainless steel and AUT surfaces

α-Syn adsorption to AUT surface was observed to be greater than to stainless steel surface as measured by both SE ($p < 0.0001$) and QCM-D ($p < 0.0001$), indicating that α-syn adsorption is surface-dependent (Fig 1). The measured SE thickness (d_{SE}) and SE mass (m_{SE}) represent the contribution of α-syn while QCM-D thickness (d_{QCMD}) and QCM-D mass (m_{QCMD}) represent both α-syn and associated DI H_2O entrapped by the α-syn layer. For stainless steel, after 1 hr of exposure to α-syn and followed by 1 hr of rinsing with DI H_2O, d_{SE} was 1.10 ± 0.07 nm and d_{QCMD} was 1.95 ± 0.30 nm (Fig 1A & 1B). Thicknesses measured for α-syn on AUT were 2.53 ± 0.72 nm (d_{SE}) and 10.68 ± 2.09 nm (d_{QCMD}), respectively (Fig 1A & 1B), which are 56% and 82% greater than adsorption on stainless steel surface, respectively. Similarly, the adsorbed mass on AUT at equilibrium were 253 ± 72 ng/cm^2 (m_{SE}) and 1,068 ± 209 ng/cm^2 (m_{QCMD}), which were 2.3 and 5.5 times greater than mass adsorption on stainless steel surface, respectively (Fig 1C & 1D).

α-Syn adsorption to stainless steel and AUT surfaces was also observed by AFM (Fig 2). After 1 hr, α-syn deposition was observed on both the stainless steel and the AUT surfaces. The increased α-syn heights observed on stainless steel surface compared with the AUT surface (Fig 2) was due to the fact that AFM images measured the largest heights while QCM-D/SE averaged α-syn thickness on the surfaces. α-Syn adsorption on the stainless

Author Manuscript Author Manuscript Author Manuscript Author Manuscript

steel surface was characterized by a punctate pattern while the α-syn deposited on the AUT surface had more fibrillar arrangement.

Attachment to both surfaces exhibited a rapid attachment stage, followed by a second stage with slower deposition, although the kinetics of attachment was different between the two surfaces. The α-syn adsorption rate for the first stage on AUT surface was 7.9 ± 3.0 ng/min cm^2, 1.1 – 2.9 times faster than on stainless steel surface (4.1 ± 0.4 ng/min cm^2), indicating that α-syn had higher affinity toward the AUT surface. The stainless steel surface reached maximum adsorption after approximately 20 mins, faster than the AUT surface, which reached maximum adsorption after 25 mins (Fig 1C & 1D).

The calculated volume fraction of α-syn on the stainless steel surface was 0.58 ± 0.04 compared with 0.23 ± 0.03 on the AUT surface.

Adsorption of α-syn onto stainless steel as a function of α-syn concentration

α-Syn orientation and conformation was dependent on the initial α-syn concentration over the concentration range from 10 μg/mL to 100 μg/mL, however, α-syn mass adsorption was not dependent on concentration (Fig 3). Based on QCM-D measurements, α-syn adsorption increased with increasing protein concentration. At equilibrium, m_{QCMD} was 196 ± 0.50 ng/cm^2, 386 ± 6.22 ng/cm^2, and 565 ± 5.50 ng/cm^2 for 10 μg/mL, 50 μg/mL, and 100 μg/mL, respectively (Fig 3B). The SE mass adsorption was comparable at various concentrations with the m_{SE} at equilibrium ranging from 102 ng/cm^2 to 110 ng/cm^2 (Fig 3).

The α-syn adsorption rates at 50 μg/mL and 100 μg/mL were faster (15.8 ng/min.cm^2 and 11.7 ng/min.cm^2, respectively) compared to 10 μg/mL (4.1 ng/min.cm^2). At 50 μg/mL and 100 μg/mL, the adsorption also reached its saturation faster than at 10 μg/mL, which were approximately 6 mins for 50 μg/mL and 100 μg/mL and 20 mins for 10 μg/mL (Fig 3B).

It was observed that the protein volume fractions on the surface varied with the initial α-syn concentration (Fig 3C). When switching to the rinsing phase, the volume fraction at 50 μg/mL and 100 μg/mL decreased while the volume fraction at 10 μg/mL was stable. The volume fractions at equilibrium were 0.56, 0.28, and 0.18 for 10 μg/mL, 50 μg/mL, and 100 μg/mL, respectively (Fig 3C), indicating that at higher concentrations, the α-syn layer was less densely compacted.

Adsorption of BSA to stainless steel

A control experiment with a non-amyloid BSA protein was conducted to demonstrate desorption capacity of 1N NaOH from contaminated surfaces using *ex-situ* SE measurement. The results from QCM-D/SE (Fig 4), *ex-situ* SE (Table 1), and AFM images (Fig 2) confirmed that the methods used in this study are suitable for testing the adsorption and desorption of α-syn on various surfaces.

BSA adsorption was 2.66 ± 0.161 nm and 5.24 ± 0.364 nm for SE and QCM-D, respectively (Fig 4A), which are approximately 2.4 and 2.7 times greater than that measured for α-syn adsorption, respectively. Mass adsorption of BSA was m_{SE} = 266 ± 16 ng/cm^2 and m_{QCMD} = 524 ± 36 ng/cm^2 (Fig 4B). The BSA adsorption rate was 11.05 ng/min cm^2 and the

Author Manuscript Author Manuscript Author Manuscript Author Manuscript

adsorption reached equilibrium after approximately 20 mins (Fig 4B). The final volume fraction of the adsorbed BSA layer was 0.51 ± 0.025 (Fig 4A).

α-syn/BSA desorption from stainless steel and AUT surfaces

The *ex-situ* measurement of the attached protein thickness before (d) and after being treated with NaOH (d_{NaOH}) was recorded in Table 1. The results showed that α-syn was completely removed from stainless steel surface ($d_{NaOH} < 0$) while a minimum amount remained on AUT surface ($d_{NaOH} > 0$). α-Syn desorption from the stainless steel and the AUT surfaces after NaOH treatment was observed from AFM images (Fig 2). AFM images obtained after NaOH treatment were similar to the stainless steel surface prior to the introduction of the protein. Similar to α-syn, BSA was completely removed after decontamination with NaOH ($d_{NaOH} < 0$, Table 1 & Fig 2).

Protein size distributions

DLS measurements of solution effluents are presented in Table 2. The average hydrodynamic diameter in the initial solutions for the stainless steel (32.8 nm) and AUT (33.7 nm) experiments was comparable. For both surfaces, it was observed that the α-syn hydrodynamic diameter distribution trended with the decreasing order of initial solution > Effluent 2 > Effluent 1. Effluent 1 (after attachment phase) contains α-syn molecules that were loosely bound or did not sorb to the surface while the Effluent 2 (after desorption phase) is expected to contain the desorbed α-syn.

Discussion

α-syn adsorption onto stainless steel and AUT surfaces

Electrostatic interactions and protein-protein interactions[64] for α-syn to surfaces were reported in a limited number of studies[30, 65, 66]. The α-syn adsorption on the stainless steel surface may be attributed to the electrostatic interaction between the positively charged regions of the N-terminal domain of α-syn to the negatively charged stainless steel surface[42, 67]. This finding is consistent with a previous study which determined that the α-syn N-terminal region could bind to anionic lipids electrostatically[42, 44]. In addition, serine residues on the N-terminal domain can bind to metal oxides on the stainless steel surface[54, 68, 69] as serine residues have a high affinity toward metal oxides such as iron oxides[70], iron ions[71, 72], and chromium oxide-hydroxides[73, 74]. Adsorption on the AUT surface could be explained by electrostatic interaction between a net negative charge of the α-syn C-terminal domain and the positively charged AUT surface[42, 67]. Since the negatively charged α-syn fibrils had greater adsorption to the positively charged AUT surface than the negatively charged stainless steel surface (Fig 1), strong electrostatic interaction is likely to be a predominant mechanism for the α-syn adsorption to the AUT surface. The fibrillar form of the adsorbed α-syn on the AUT surface compared to the punctate pattern observed on the stainless steel surface can also explain differences of the orientation and conformation of α-syn on the two surfaces (Fig 2) Fibrillar α-syn was observed on the AUT surface after 1 hour of adsorption, suggesting that the positive amine ($–NH_2$) tail group of the AUT surface promote α-syn fibril aggregation while the negatively charged stainless steel surface does not. Alternatively, oligomeric or small fibrillar α-syn may preferentially bind to the stainless

Author Manuscript Author Manuscript Author Manuscript Author Manuscript

steel surface or α-syn fibrils are fragmented upon binding to the stainless steel surface due to the metal-protein interaction, resulting fewer α-syn fibrils on the stainless steel surface. Dissipation shifts (ΔD > 0) (Fig S2) obtained from the QCM-D measurements for α-syn adsorption on AUT surface indicated that the adsorbed α-syn layer on the surfaces was a soft and viscoelastic layer[60, 61], which is different from the rigid film of α-syn and BSA adsorbed on the stainless steel surface (ΔD ~ 0) (Fig S1). Formation of a rigid film for BSA adsorption was reported in a previous study by the authors using a similar QCM-D/SE technique[41], which confirms the validity and suitability of the methods and techniques used in this study.

α-Syn adsorbed on the AUT had a lower volume fraction than for the stainless steel surface, indicating that it is less densely compacted. Alternately, there were more DI H_2O molecules entrapped within the α-syn layer adsorbed on the AUT surface, which might be attributed to the fibrillar-like structure on the AUT surface (Fig 2), compared to α-syn on the stainless steel surface. Since the DI H_2O molecules are more favorably attracted by the charged amino acids on the C-terminal domain (10 Glu and 5 Asp residues) and the N-terminal domain (Lys residues) of α-syn[42], more C- and N-terminal domains in the fibrillar structure could result in more DI H_2O molecules entrapped within these two domains. In addition, the highly hydrophobic central region of α-syn fibrils in AUT adsorption is less exposed to the ambient DI H_2O than free α-syn oligomers or small fibrils in stainless steel adsorption. This explains the higher adsorbate fraction for the stainless steel surface ($f_{o,V}$ = 0.56) and lower adsorbate fraction for the AUT surface ($f_{o,V}$ = 0.24).

α-syn adsorption onto stainless steel as a function of α-syn concentration

Influence of α-syn concentration on its adsorption to stainless steel surfaces has not been studied before. In this study, the initial aqueous α-syn concentration had influence on α-syn orientation and conformation on the stainless steel surface but did not influence α-syn mass adsorption. The m_{SE} are comparable for various concentration but m_{QCMD} increased with increasing concentration (Fig 3), indicating that the initial protein concentration influenced the arrangement of α-syn on the surface, but did not affect the mass of protein adsorbed. The attached protein layer had a greater porosity (lower $f_{o,V}$), resulting in lower compacted density, with increasing α-syn concentration. This indicates that higher protein concentration leads to more ambient DI H_2O association with the adsorbate. At equilibrium, the layer porosity increased 69.3% and 69.8% for 50 μg/mL 100 μg/mL, respectively, indicating that rinsing with DI H_2O facilitated the conformational change of α-syn on the stainless steel surface. However, at 10 μg/mL, the adsorbed α-syn conformation was minimally changed (0.6%) as demonstrated by the stable volume fraction ($f_{o,V}$) in the rinsing phase (Fig 3).

α-syn desorption from stainless steel and AUT surfaces

1N NaOH solution completely or partially removed adsorbed α-syn on stainless steel and AUT surfaces, respectively. The results were consistent for both *ex-situ* SE measurement and AFM images (Fig 2 & Table 1). The strong decontamination activity of NaOH were previously studied in sterilization of prion contaminated surfaces[22, 26, 27, 75-77]. 1N NaOH was recommended as a candidate reagent for decontamination of prions from stainless steel

Author Manuscript Author Manuscript Author Manuscript Author Manuscript

surfaces in which the *in-vitro* experiment was conducted under the similar conditions to this study[78]. In addition, the ability of 1N NaOH to promote complete removal of α-syn from stainless steel wires previously reported in a study under similar treatment conditions using Western blot[21] confirmed the validity and suitability of the methods used in this study. However, in the previous report, the decontamination was determined qualitatively while in this study, quantitative removal of adsorbed α-syn was obtained, especially the extent of partial removal of α-syn adsorbed on AUT surface (Table 1). Stainless steel surface metal release (e.g. iron, chromium, nickel)[69, 79, 80] may occur along with the decontamination of adsorbed a-syn, which contributes to desorption from the stainless steel surface and could explain the negative thickness (d_{NaOH}) observed after desorption (Table 1).

Protein desorption efficacy from stainless steel surfaces was also reported in another study using various NaOH concentration[81]. Na^+ and OH^- ions could change surface pH or interfere with surface-protein binding leading to protein desorption[79]. The removal efficiency of α-syn from the stainless steel surface is greater than that from the AUT surface regardless of the α-syn concentration (Table 1), indicating that removal efficiency is more likely to depend on the surface-protein binding and the adsorbed α-syn structure than protein-protein binding. The larger α-syn aggregation of fibrils might be more difficult to be removed by NaOH solution compared to free α-syn smaller fibrils, indicating that the binding of the α-syn fibrils to the AUT surface is stronger than the stainless steel surface. It can also be inferred that the 1N NaOH could exert the detaching and the destabilizing effect on the protein[78] adsorbed to the AUT surface and the degrading effect on the stainless steel surface. The result is of importance in environmental decontamination since AUT surfaces mimic environmental surfaces. Since α-syn is a prion-like protein[7-9], environmental surfaces contaminated with α-syn would be very difficult to decontaminate and α-syn-contaminated environmental surfaces could also be resistant to most of inactivation treatments in a similar fashion to prion-contaminated surfaces[16, 18, 22-28].

α-syn size distribution

For the stainless steel surface, protein with sizes greater than 20 nm were not detected in Effluent 1, indicating that these particle sizes preferentially adsorbed to the surface leaving the smaller α-syn molecules (< 20 nm) free in the effluent. The average hydrodynamic diameter of the initial solution was 32.8 nm, but the diameter in Effluent 1 was only 3.4 nm. That the appearance of the α-syn particle size range of 10 – 20 nm in Effluent 1 was not detected in the initial solution could be explained due to several reasons: (1) larger α-syn fibrils might be broken during adsorption; or (2) adsorbed α-syn can seed conformational changes in free α-syn[30]. Desorption of α-syn from the stainless steel surface after NaOH treatment is confirmed by the increase in the average hydrodynamic diameter of α-syn in Effluent 2 (22 nm). The predominant particle size distribution in Effluent 2 was between 2 and 5 nm. The greater fraction of smaller particles in Effluent 2 may indicate that NaOH reduces the α-syn particle sizes during the desorption process. Conversely, there was less change in the particle size distributions for α-syn after adsorption to AUT (Effluent 1) and after decontamination with NaOH (Effluent 2). For the AUT surface, the average hydrodynamic diameter did not change considerably from the initial solution in the case of either effluent.

Author Manuscript Author Manuscript Author Manuscript Author Manuscript

Conclusions

Adsorption and decontamination of α-syn fibrils to stainless steel and AUT surfaces were examined using QCM-D/SE, AFM imaging, and DLS measurements. We determined that α-syn can bind to multiple surface types and that the orientation, conformation, and decontamination of α-syn is surface-dependent. α-Syn had greater adsorption and lower compactness on the AUT surface when compared to the stainless steel surface. Changes in protein orientation on the two surfaces were observed with rigid sub-monolayers formation on the stainless steel surfaces and viscous layer on the AUT surface. The large α-syn preferentially adsorbed to the stainless steel surface as individual oligomers or small fibrils while the adsorption on the AUT surface is more as random aggregations or conformations of larger α-syn fibrils. The α-syn had greater affinity toward the AUT surface compared to the stainless steel surface. The electrostatic interactions are mainly responsible for the α-syn adsorption. α-syn concentration affects conformation and orientation but do not affect areal mass of adsorbed α-syn on the stainless steel surface. 1N NaOH solution decontaminated the stainless steel surfaces better than the AUT surface. These results are relevant to develop practices of reliably decontaminate medically or environmentally contaminated surfaces. As α-syn and prions shares many neuropathogenic traits, especially their ability of iatrogenic transmission of MSA or prion disease, most hospital sterilization methods will be ineffective. Our finding suggested 1N NaOH solution for contaminated stainless steel surgical tools decontamination. Excessive care must be considered about α-syn contamination on the environmental surfaces as from our results, α-syn bound to environmental surfaces survived after NaOH decontamination. Future studies are to establish effective methods to sterilize contaminated α-syn in the environment.

Supplementary Material

Refer to Web version on PubMed Central for supplementary material.

Acknowledgments

We thank Dr. Lanping Yue (Nebraska Center for Materials and Nanoscience) for AFM imaging training and professional advice on AFM image analysis. The research was performed in part in the Nebraska Nanoscale Facility: National Nanotechnology Coordinated Infrastructure and the Nebraska Center for Materials and Nanoscience, which are supported by the National Science Foundation under Award ECCS: 1542182, and the Nebraska Research Initiative.

FUNDING

Funding for this work was provided in part by funds from the Center for Nanohybrid Functional Materials through an award to MS (NSF-EPS-10004094), to SLB (NSF CBET-1149424) and to BIG (NIH R01NS089622).

References

1. Goedert M. Alpha-synuclein and neurodegenerative diseases. Nature Reviews Neuroscience. 2001; 2(7):492–501. [PubMed: 11433374]
2. Spillantini MG, Schmidt ML, Lee VMY, Trojanowski JQ, Jakes R, Goedert M. Alpha-synuclein in Lewy bodies. Nature. 1997; 388(6645):839–840. [PubMed: 9278044]
3. Baba M, Nakajo S, Tu PH, Tomita T, Nakaya K, Lee VMY, Trojanowski JQ, Iwatsubo T. Aggregation of alpha-synuclein in Lewy bodies of sporadic Parkinson's disease and dementia with lewy bodies. American Journal of Pathology. 1998; 152(4):879–884. [PubMed: 9546347]

Author Manuscript Author Manuscript Author Manuscript Author Manuscript

4. Wakabayashi K, Yoshimoto M, Tsuji S, Takahashi H. Alpha-synuclein immunoreactivity in glial cytoplasmic inclusions in multiple system atrophy. Neuroscience Letters. 1998; 249(2–3):180–182. [PubMed: 9682846]
5. Xu L, Ma B, Nussinov R, Thompson D. Familial mutations may switch conformational preferences in α-synuclein fibrils. ACS Chemical Neuroscience. 2017
6. Petrucci S, Ginevrino M, Valente EM. Phenotypic spectrum of alpha-synuclein mutations: New insights from patients and cellular models. Parkinsonism & Related Disorders. 2016; 22:S16–S20. [PubMed: 26341711]
7. Aulic S, Le TTN, Moda F, Abounit S, Corvaglia S, Casalis L, Gustincich S, Zurzolo C, Tagliavini F, Legname G. Defined alpha-synuclein prion-like molecular assemblies spreading in cell culture. Bmc Neuroscience. 2014; 15:12. [PubMed: 24423059]
8. Olanow CW, Brundin P. Parkinson's Disease and Alpha Synuclein: Is Parkinson's Disease a Prion-Like Disorder? Movement Disorders. 2013; 28(1):31–40. [PubMed: 23390095]
9. Masuda-Suzukake M, Nonaka T, Hosokawa M, Oikawa T, Arai T, Akiyama H, Mann DMA, Hasegawa M. Prion-like spreading of pathological alpha-synuclein in brain. Brain. 2013; 136:1128–1138. [PubMed: 23466394]
10. Prusiner, SB. An introduction to prion biology and diseases. In: Prusiner, SB., editor. Biology and Diseases. Cold Spring Harbor Laboratory Press; Cold Spring Harbor, NY: 2004.
11. Polymenidou M, Cleveland DW. Prion-like spread of protein aggregates in neurodegeneration. Journal of Experimental Medicine. 2012; 209(5):889–893. [PubMed: 22566400]
12. Sacino AN, Brooks M, Thomas MA, McKinney AB, Lee S, Regenhardt RW, McGarvey NH, Ayers JI, Notterpek L, Borchelt DR, Golde TE, Giasson BI. Intramuscular injection of alpha-synuclein induces CNS alpha-synuclein pathology and a rapid-onset motor phenotype in transgenic mice. Proceedings of the National Academy of Sciences of the United States of America. 2014; 111(29): 10732–10737. [PubMed: 25002524]
13. Breid S, Bernis ME, Babila JT, Garza MC, Wille H, Tamguney G. Neuroinvasion of alpha-Synuclein Prionoids after Intraperitoneal and Intraglossal Inoculation. Journal of Virology. 2016; 90(20):9182–9193. [PubMed: 27489279]
14. Peelaerts W, Bousset L, Van der Perren A, Moskalyuk A, Pulizzi R, Giugliano M, Van den Haute C, Melki R, Baekelandt V. Alpha-Synuclein strains cause distinct synucleinopathies after local and systemic administration. Nature. 2015; 522(7556):340. -+ [PubMed: 26061766]
15. Secker TJ, Herve R, Keevil CW. Adsorption of prion and tissue proteins to surgical stainless steel surfaces and the efficacy of decontamination following dry and wet storage conditions. Journal of Hospital Infection. 2011; 78(4):251–255. [PubMed: 21658801]
16. Zobeley E, Flechsig E, Cozzio A, Enari M, Weissmann C. Infectivity of scrapie prions bound to a stainless steel surface. Molecular Medicine. 1999; 5(4):240–243. [PubMed: 10448646]
17. Bernoulli C, Siegfried J, Baumgartner G, Regli F, Rabinowicz T, Gajdusek DC, Gibbs CJ. Danger of accidental person to person transmission of Creutzfeldt-Jakob disease by surgery. Lancet. 1977; 1(8009):478–479. [PubMed: 65575]
18. Gibbs CJ, Asher DM, Kobrine A, Amyx HL, Sulima MP, Gajdusek DC. Transmission of Creutzfeldt-Jakob disease to a chimpanzee by electrodes contaminated during neurosurgery. Journal of Neurology Neurosurgery and Psychiatry. 1994; 57(6):757–758.
19. Furtner M, Gelpi E, Kiechl S, Knoflach M, Zangerl A, Gotwald T, Willeit J, Maier H, Strobel T, Unterberger U, Budka H. Iatrogenic Creutzfeldt-Jakob disease 22 years after human growth hormone therapy: clinical and radiological features. Journal of Neurology Neurosurgery and Psychiatry. 2008; 79(2):229–231.
20. Will RG. Acquired prion disease: iatrogenic CJD, variant CJD, kuru. British Medical Bulletin. 2003; 66:255–265. [PubMed: 14522863]
21. Thomzig A, Wagenführ K, Daus ML, Joncic M, Schulz-Schaeffer WJ, Thanheiser M, Mielke M, Beekes M. Decontamination of medical devices from pathological amyloid-β-, tau- and α-synuclein aggregates. Acta Neuropathologica Communications. 2014; 2(151)
22. Flechsig E, Hegyi I, Enari M, Schwarz P, Collinge J, Weissmann C. Transmission of scrapie by steel-surface-bound prions. Molecular Medicine. 2001; 7(10):679–684. [PubMed: 11713367]

Author Manuscript Author Manuscript Author Manuscript Author Manuscript

23. Alper T, Haig DA, Clarke MC. Exceptionally small size of scrapie agent. Biochemical and Biophysical Research Communications. 1966; 22(3):278–284. [PubMed: 4957205]
24. Gibbs CJ, Gajdusek DC, Latarjet R. Unusual resistance to ionizing-radiation of the viruses of Kuru, Creutzfeldt-Jakob disease, and scrapie. Proceedings of the National Academy of Sciences of the United States of America. 1978; 75(12):6268–6270. [PubMed: 104301]
25. Ernst DR, Race RE. Comparative-analysis of scrapie agent inactivation methods. Journal of Virological Methods. 1993; 41(2):193–201. [PubMed: 8496294]
26. Taylor DM, Fraser H, McConnell I, Brown DA, Brown KL, Lamza KA, Smith GRA. Decontamination studies with the agents of bovine spongiform encephalopathy and scrapie. Archives of Virology. 1994; 139(3–4):313–326. [PubMed: 7832638]
27. Taylor DM. Inactivation of transmissible degenerative encephalopathy agents: A review. Veterinary Journal. 2000; 159(1):10–17.
28. Brown P, Gibbs CJ, Amyx HL, Kingsbury DT, Rohwer RG, Sulima MP, Gajdusek DC. Chemical disinfection of Creutzfeldt-Jakob disease virus. New England Journal of Medicine. 1982; 306(21): 1279–1282. [PubMed: 7040968]
29. Woerman AL, Kazmi SA, Patel S, Freyman Y, Oehler A, Aoyagi A, Mordes DA, Halliday GM, Middleton LT, Gentleman SM, Olson SH, Prusiner SB. MSA prions exhibit remarkable stability and resistance to inactivation. Acta Neuropathol. 2017:1–15.
30. Yang JA, Lin W, Woods WS, George JM, Murphy CJ. alpha-Synuclein's Adsorption, Conformation, and Orientation on Cationic Gold Nanoparticle Surfaces Seeds Global Conformation Change. Journal of Physical Chemistry B. 2014; 118(13):3559–3571.
31. Yang JA, Johnson BJ, Wu S, Woods WS, George JM, Murphy CJ. Study of Wild-Type alpha-Synuclein Binding and Orientation on Gold Nanoparticles. Langmuir. 2013; 29(14):4603–4615. [PubMed: 23477540]
32. Brown P, Rau EH, Lemieux P, Johnson BK, Bacote AE, Gajdusek DC. Infectivity studies of both ash and air emissions from simulated incineration of scrapie-contaminated tissues. Environmental Science & Technology. 2004; 38(22):6155–6160. [PubMed: 15575075]
33. Greig JR, Serapie. Observations on the Transmission of the Disease by Mediate Contact. Vet J. 1940; 96:203–206.
34. Hadlow WJ, Kennedy RC, Race RE. Natural infection of suffolk sheep with scrapie virus. Journal of Infectious Diseases. 1982; 146(5):657–664. [PubMed: 6813384]
35. Miller MW, Williams ES. Prion disease: horizontal prion transmission in mule deer. Nature. 2003; 425(6953):35–6. [PubMed: 12955129]
36. Miller MW, Williams ES, Hobbs NT, Wolfe LL. Environmental Sources of Prion Transmission in Mule Deer. Emerging Infectious DiseasesEmerging Infectious Diseases. 2004; 10(6):1003–1006.
37. Bessen RA, Marsh RF. Distinct PrP properties suggest the molecular-basis of strain variation in transmissible mink encephalopathy. Journal of Virology. 1994; 68(12):7859–7868. [PubMed: 7966576]
38. Mathiason CK, Powers JG, Dahmes SJ, Osborn DA, Miller KV, Warren RJ, Mason GL, Hays SA, Hayes-Klug J, Seelig DM, Wild MA, Wolfe LL, Spraker TR, Miller MW, Sigurdson CJ, Telling GC, Hoover EA. Infectious prions in the saliva and blood of deer with chronic wasting disease. Science. 2006; 314(5796):133–136. [PubMed: 17023660]
39. Voinova MV, Rodahl M, Jonson M, Kasemo B. Viscoelastic acoustic response of layered polymer films at fluid-solid interfaces: Continuum mechanics approach. Physica Scripta. 1999; 59(5):391–396.
40. Carton I, Brisson AR, Richter RP. Label-Free Detection of Clustering of Membrane-Bound Proteins. Analytical Chemistry. 2010; 82(22):9275–9281. [PubMed: 21028837]
41. Phan H, Bartelt-Hunt S, Rodenhausen K, Schubert M, Bart J. Investigation of Bovine Serum Albumin (BSA) Attachment onto Self-Assembled Monolayers (SAMs) Using Combinatorial Quartz Crystal Microbalance with Dissipation (QCM-D) and Spectroscopic Ellipsometry (SE). PLoS ONE. 2015; 10(10):e0141282. [PubMed: 26505481]
42. Emamzadeh FN. Alpha-synuclein structure, functions, and interactions. Journal of Research in Medical Sciences. 2016; 21(2):165–173.

Author Manuscript Author Manuscript Author Manuscript Author Manuscript

43. Hoyer W, Antony T, Cherny D, Heim G, Jovin TM, Subramaniam V. Dependence of alpha-synuclein aggregate morphology on solution conditions. Journal of Molecular Biology. 2002; 322(2):383–393. [PubMed: 12217698]
44. Pfefferkorn CM, Jiang ZP, Lee JC. Biophysics of alpha-synuclein membrane interactions. Biochimica Et Biophysica Acta-Biomembranes. 2012; 1818(2):162–171.
45. Weinreb PH, Zhen WG, Poon AW, Conway KA, Lansbury PT. NACP, a protein implicated in Alzheimer's disease and learning, is natively unfolded. Biochemistry. 1996; 35(43):13709–13715. [PubMed: 8901511]
46. Rajagopalan S, Andersen JK. Alpha synuclein aggregation: is it the toxic gain of function responsible for neurodegeneration in Parkinson's disease? Mechanisms of Ageing and Development. 2001; 122(14):1499–1510. [PubMed: 11511392]
47. Rodriguez JA, Ivanova MI, Sawaya MR, Cascio D, Reyes FE, Shi D, Sangwan S, Guenther EL, Johnson LM, Zhang M, Jiang L, Arbing MA, Nannenga BL, Hattne J, Whitelegge J, Brewster AS, Messerschmidt M, Boutet B, Sauter NK, Gonen T, Eisenberg DS. Structure of the toxic core of alpha-synuclein from invisible crystals. Nature. 2015; 525(7570):486. -+ [PubMed: 26352473]
48. Uversky VN. Neuropathology, biochemistry, and biophysics of alpha-synuclein aggregation. Journal of Neurochemistry. 2007; 103(1):17–37. [PubMed: 17623039]
49. Uversky VN, Li J, Fink AL. Evidence for a partially folded intermediate in alpha-synuclein fibril formation. Journal of Biological Chemistry. 2001; 276(14):10737–10744. [PubMed: 11152691]
50. Waxman EA, Mazzulli JR, Giasson BI. Characterization of Hydrophobic Residue Requirements for alpha-Synuclein Fibrillization. Biochemistry. 2009; 48(40):9427–9436. [PubMed: 19722699]
51. Giasson BI, Murray IVJ, Trojanowski JQ, Lee VMY. A hydrophobic stretch of 12 amino acid residues in the middle of alpha-synuclein is essential for filament assembly. Journal of Biological Chemistry. 2001; 276(4):2380–2386. [PubMed: 11060312]
52. Crystal AS, Giasson BI, Crowe A, Kung MP, Zhuang ZP, Trojanowski JQ, Lee VMY. A comparison of amyloid fibrillogenesis using the novel fluorescent compound K114. Journal of Neurochemistry. 2003; 86(6):1359–1368. [PubMed: 12950445]
53. Peters, TJ. All About Albumin: Biochemistry, Genetics, and Medical Applications. Academic Press; San Diego, CA: p. 1996
54. Chandrasekaran N, Dimartino S, Fee CJ. Study of the adsorption of proteins on stainless steel surfaces using QCM-D. Chemical Engineering Research & Design. 2013; 91(9):1674–1683.
55. Chong KSL, Sun SQ, Leggett GJ. Measurement of the kinetics of photo-oxidation of self-assembled monolayers using friction force microscopy. Langmuir. 2005; 21(9):3903–3909. [PubMed: 15835953]
56. Love JC, Estroff LA, Kriebel JK, Nuzzo RG, Whitesides GM. Self-assembled monolayers of thiolates on metals as a form of nanotechnology. Chemical Reviews. 2005; 105(4):1103–1169. [PubMed: 15826011]
57. Bradford DC, Hutter E, Fendler JH, Roy D. Surface-enhanced infrared ellipsometry of self-assembled undecanethiol and dodecanethiol monolayers on disordered gold nanoisland substrates. Journal of Physical Chemistry B. 2005; 109(44):20914–20922.
58. Rodenhausen KB, Schubert M. Virtual separation approach to study porous ultra-thin films by combined spectroscopic ellipsometry and quartz crystal microbalance methods. Thin Solid Films. 2011; 519(9):2772–2776.
59. Rodenhausen KB, Duensing BA, Kasputis T, Pannier AK, Hofmann T, Schubert M, Tiwald TE, Solinsky M, Wagner M. *In-situ* monitoring of alkanethiol self-assembled monolayer chemisorption with combined spectroscopic ellipsometry and quartz crystal microbalance techniques. Thin Solid Films. 2011; 519(9):2817–2820.
60. Kananizadeh N, Rice C, Lee J, Rodenhausen KB, Sekora D, Schubert M, Schubert E, Bartelt-Hunt S, Li YS. Combined quartz crystal microbalance with dissipation (QCM-D) and generalized ellipsometry (GE) to characterize the deposition of titanium dioxide nanoparticles on model rough surfaces. Journal of Hazardous Materials. 2017; 322:118–128. [PubMed: 27041442]
61. Reviakine I, Johannsmann D, Richter RP. Hearing What You Cannot See and Visualizing What You Hear: Interpreting Quartz Crystal Microbalance Data from Solvated Interfaces. Analytical Chemistry. 2011; 83(23):8838–8848. [PubMed: 21939220]

Author Manuscript Author Manuscript Author Manuscript Author Manuscript

62. Kasputis T, Pieper A, Schubert M, Pannier AK. Dynamic Analysis of DNA Nanoparticle Immobilization to Model Biomaterial Substrates Using Combinatorial Spectroscopic Ellipsometry and Quartz Crystal Microbalance with Dissipation. Thin Solid Films. 2014; 571(3):637–643.
63. Chen KL, Elimelech M. Aggregation and Deposition Kinetics of Fullerene (C60) Nanoparticles. Langmuir. 2006; 22:10994–11001. [PubMed: 17154576]
64. Dedmon MM, Lindorff-Larsen K, Christodoulou J, Vendruscolo M, Dobson CM. Mapping long-range interactions in alpha-synuclein using spin-label NMR and ensemble molecular dynamics simulations. Journal of the American Chemical Society. 2005; 127(2):476–477. [PubMed: 15643843]
65. Fernandez CO, Hoyer W, Zweckstetter M, Jares-Erijman EA, Subramaniam V, Griesinger C, Jovin TM. NMR of alpha-synuclein-polyamine complexes elucidates the mechanism and kinetics of induced aggregation. Embo Journal. 2004; 23(10):2039–2046. [PubMed: 15103328]
66. Bertoncini CW, Jung YS, Fernandez CO, Hoyer W, Griesinger C, Jovin TM, Zweckstetter M. Release of long-range tertiary interactions potentiates aggregation of natively unstructured alpha-synuclein. Proceedings of the National Academy of Sciences of the United States of America. 2005; 102(5):1430–1435. [PubMed: 15671169]
67. Azucena G-H, Brenda H, Abelardo C-M. Fluorescence as a Tool to Study Lipid-Protein Interactions: The Case of α-Synuclein. Open Journal of Biophysics. 2013; 3(1A):112–119.
68. Shi J, Hedberg Y, Lundin M, Wallinder IO, Karlsson HL, Moller L. Hemolytic properties of synthetic nano- and porous silica particles: The effect of surface properties and the protection by the plasma corona. Acta Biomaterialia. 2012; 8(9):3478–3490. [PubMed: 22522009]
69. Lundin M, Hedberg Y, Jiang T, Herting G, Wang X, Thormann E, Blomberg E, Wallinder IO. Adsorption and protein-induced metal release from chromium metal and stainless steel. Journal of Colloid and Interface Science. 2012; 366(1):155–164. [PubMed: 22014396]
70. Suci PA, Geesey GG. Comparison of adsorption behavior of two Mytilus edulis foot proteins on three surfaces. Colloids and Surfaces B-Biointerfaces. 2001; 22(2):159–168.
71. Bernos E, Girardet JM, Humbert G, Linden G. Role of the O-phosphoserine clusters in the interaction of the bovine milk alpha(s1)-, beta-, kappa-caseins and the PP3 component with immobilized iron(III) ions. Biochimica Et Biophysica Acta-Protein Structure and Molecular Enzymology. 1997; 1337(1):149–159.
72. Stewart RJ, Ransom TC, Hlady V. Natural Underwater Adhesives. Journal of Polymer Science Part B-Polymer Physics. 2011; 49(11):757–771.
73. Degenhardt J, McQuillan AJ. Mechanism of oxalate ion adsorption on chromium oxide-hydroxide from pH dependence and time evolution of ATR-IR spectra. Chemical Physics Letters. 1999; 311(3–4):179–184.
74. Connor PA, McQuillan AJ. Phosphate adsorption onto TiO2 from aqueous solutions: An in situ internal reflection infrared spectroscopic study. Langmuir. 1999; 15(8):2916–2921.
75. Brown P, Rohwer RG, Gajdusek DC. Newer data on the inactivation of scrapie virus or Creutzfeldt-Jakob disease virus in brain-tissuse. Journal of Infectious Diseases. 1986; 153(6): 1145–1148. [PubMed: 3084671]
76. Kimberlin RH, Walker CA, Millson GC, Taylor DM, Robertson PA, Tomlinson AH, Dickinson AG. Disinfection studies with 2 strains of mouse-passaged scrapie agent - Guidelines for Creutzfeldt-Jakob and related agents. Journal of the Neurological Sciences. 1983; 59(3):355–369. [PubMed: 6308174]
77. Rutala WA, Weber DJ. Creutzfeldt-Jakob disease: Recommendations for disinfection and sterilization. Clinical Infectious Diseases. 2001; 32(9):1348–1356. [PubMed: 11303271]
78. Lemmer K, Mielke M, Pauli G, Beekes M. Decontamination of surgical instruments from prion proteins: in vitro studies on the detachment, destabilization and degradation of PrPSc bound to steel surfaces. Journal of General Virology. 2004; 85:3805–3816. [PubMed: 15557254]
79. Hedberg Y, Wang X, Hedberg J, Lundin M, Blomberg E, Wallinder IO. Surface-protein interactions on different stainless steel grades: effects of protein adsorption, surface changes and metal release. Journal of Materials Science-Materials in Medicine. 2013; 24(4):1015–1033. [PubMed: 23378148]
80. Hedberg YS, Killian MS, Blomberg E, Virtanen S, Schmuki P, Wallinder IO. Interaction of Bovine Serum Albumin and Lysozyme with Stainless Steel Studied by Time-of-Flight Secondary Ion

Author Manuscript Author Manuscript Author Manuscript Author Manuscript

Mass Spectrometry and X-ray Photoelectron Spectroscopy. Langmuir. 2012; 28(47):16306–16317. [PubMed: 23116183]

81. Itoh H, Nagai T, Saeki T, Sakiyama T, Nakanishi K. Adsorption of protein onto stainless steel particle surface and its desorption behavior. Developments in Food Engineering, Pts 1 and 2: Proceedings of the 6th International Congress on Engineering and Food. 1994:811–813.

Author Manuscript Author Manuscript Author Manuscript Author Manuscript

Highlights

- α-Synuclein adsorption was surface-dependent.
- Decontamination was more effective on the medical surface
- Larger α-synuclein oligomers adsorbed to the medical surface

Author Manuscript Author Manuscript Author Manuscript Author Manuscript

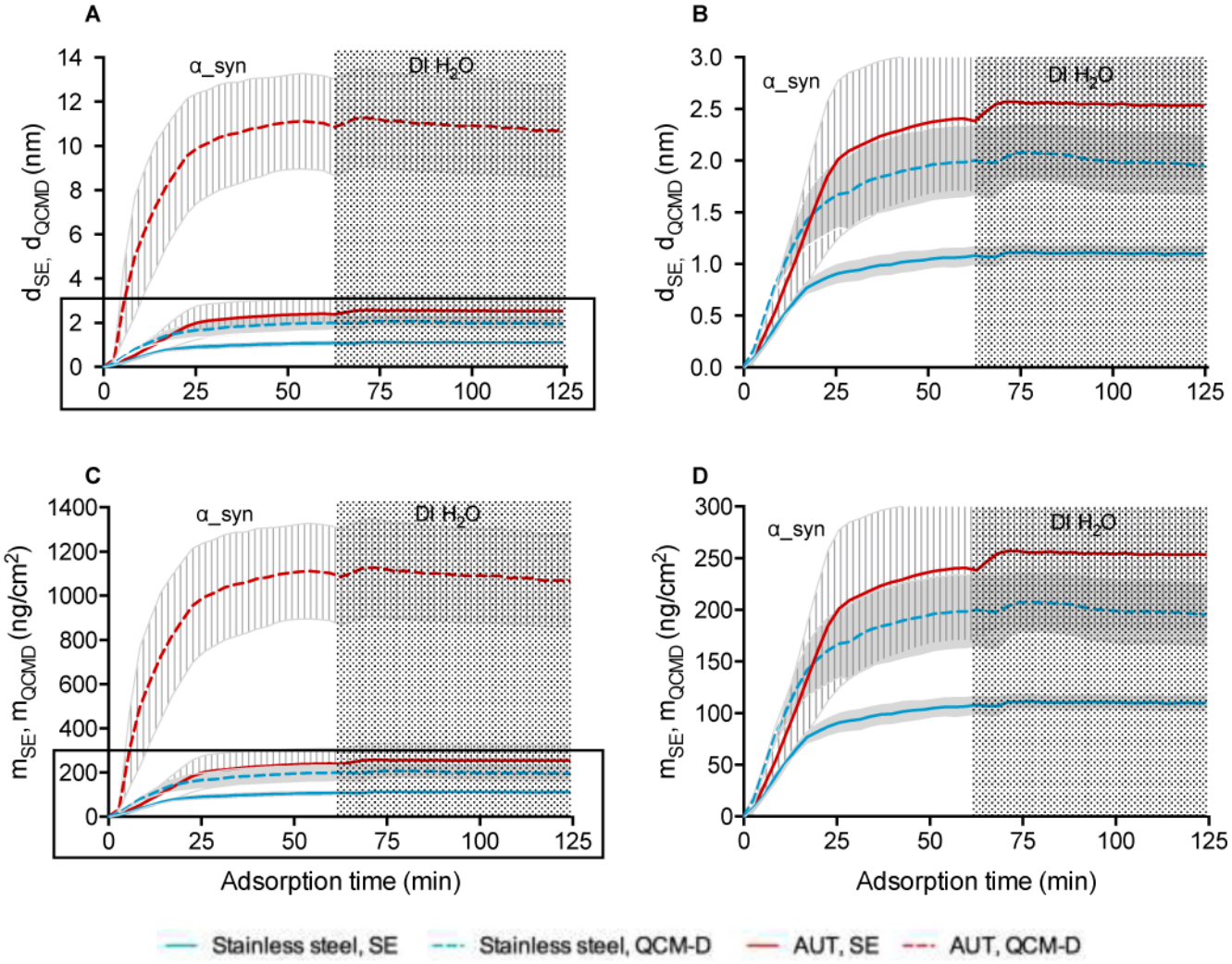

Figure 1.

α-syn adsorption on stainless steel and AUT surfaces. A) Thickness; B) Zoom in of the box in A; C) Areal mass; D) Zoom in of the box in C. Shaded areas indicated standard error of the mean (SEM) for stainless steel and AUT (n = 3).

Author Manuscript Author Manuscript Author Manuscript Author Manuscript

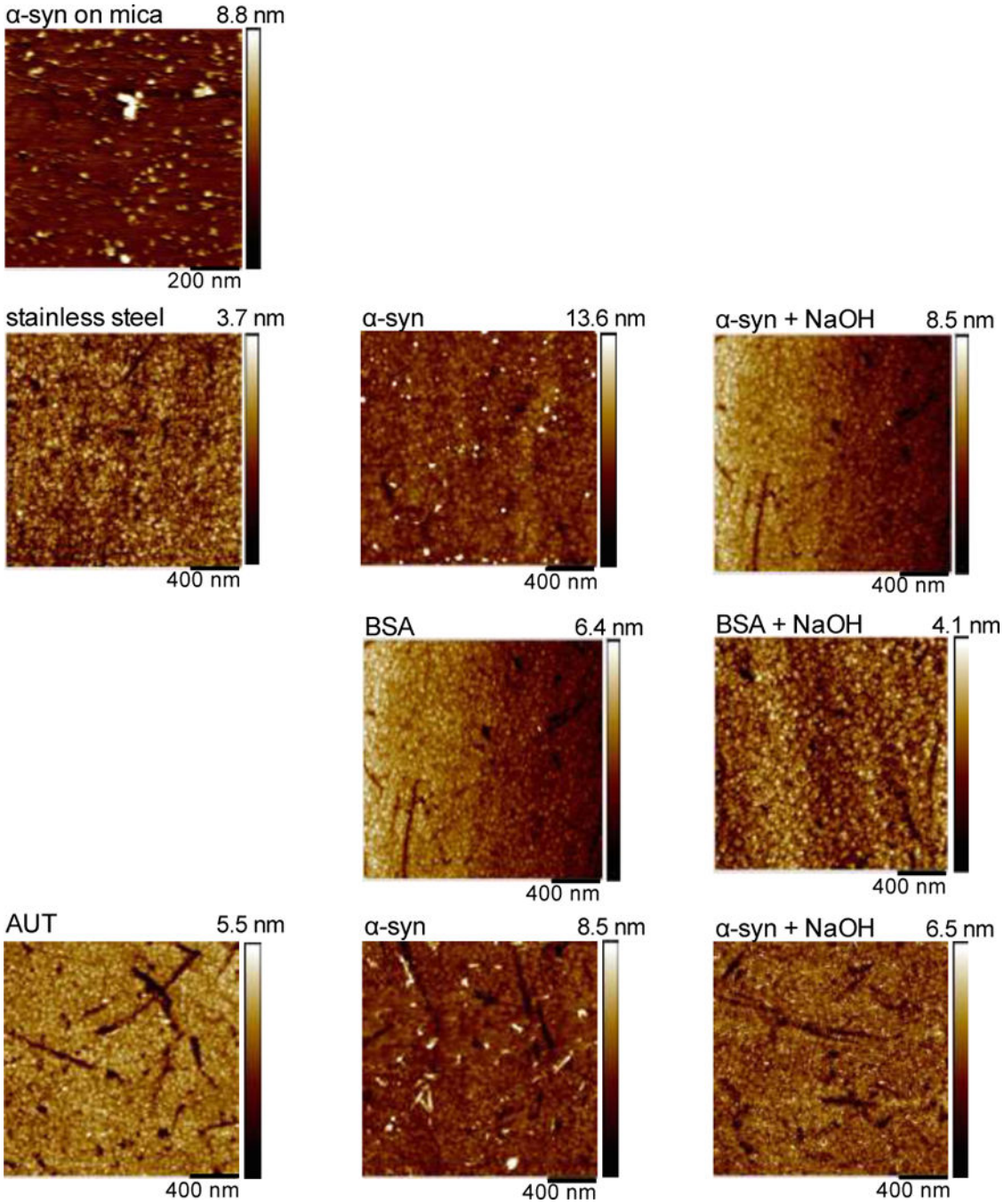

Figure 2.

Representative AFM images. First row, AFM image of α-syn 10 μg/mL on mica. Similar AFM image result of α-syn on mica was reported in previous study[7]. Second and third rows, AFM image of fresh stainless steel surface, and representative AFM images of α-syn 10 μg/mL and BSA 10 μg/mL on stainless steel with and without being treated with 1N NaOH. Last row, AFM image of AUT adsorbed on Au surface, and representative AFM images of α-syn 10 μg/mL on AUT surface with and without being treated with 1N NaOH.

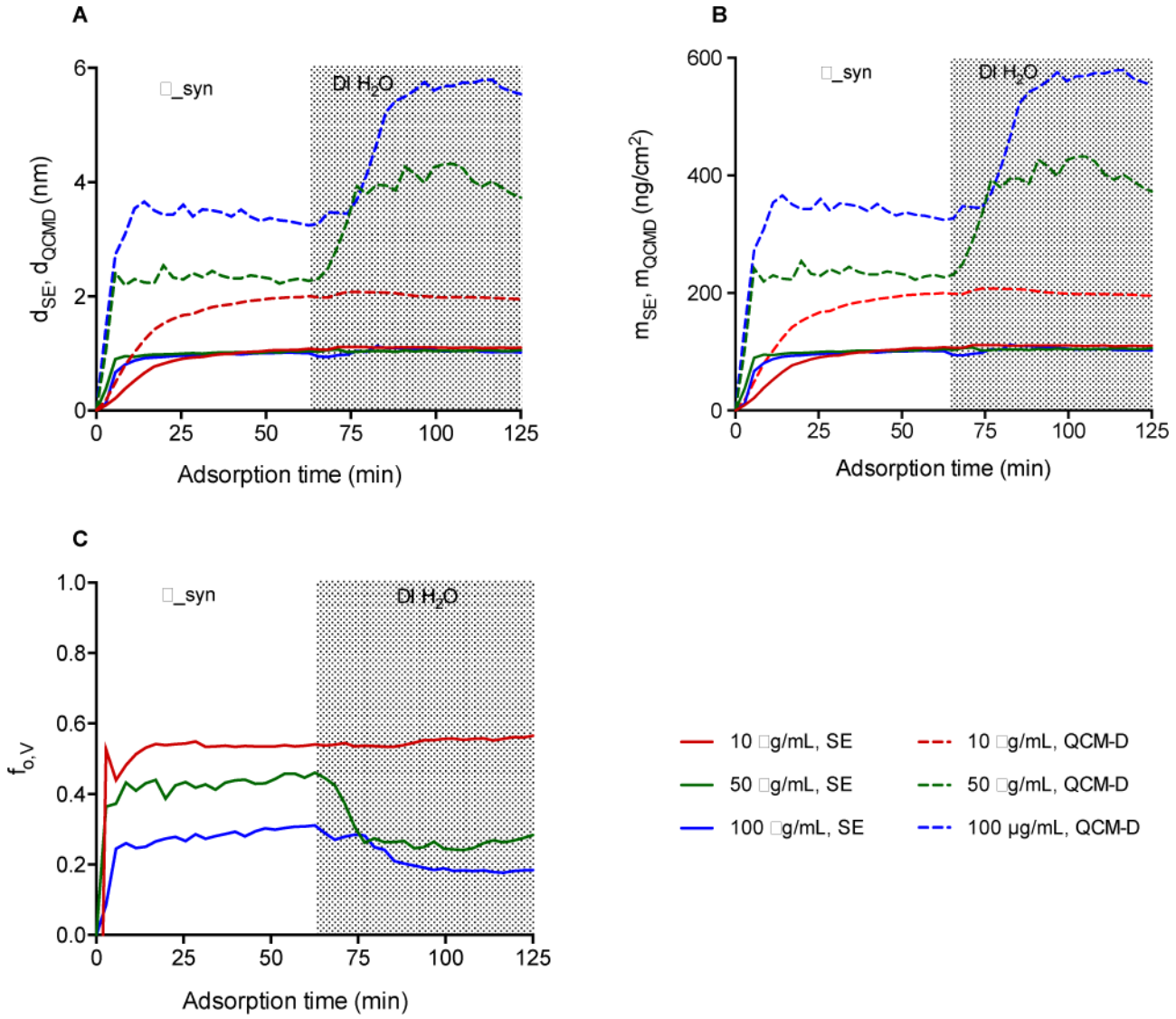

Figure 3.

Representative plot of α-syn adsorption at 10 µg/mL, 50 µg/mL, and 100 µg/mL on stainless steel surfaces: A) Thickness; B) Areal mass; C) Volume fraction.

Author Manuscript Author Manuscript Author Manuscript Author Manuscript

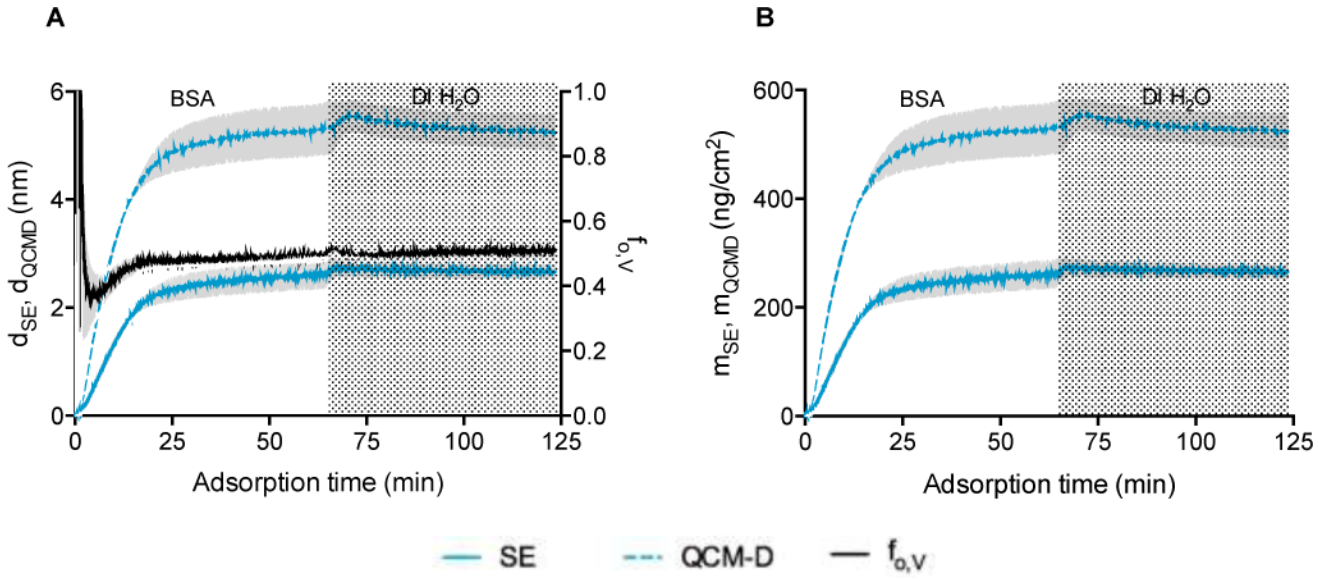

Figure 4.

BSA adsorption on stainless steel. A) Thickness and volume fraction; B) Areal mass. Shaded areas indicated relevant standard error of the mean (SEM) (n = 3).

Author Manuscript Author Manuscript Author Manuscript Author Manuscript

Author Manuscript Author Manuscript Author Manuscript Author Manuscript

Table 1

Ex-situ measurements of α-syn and BSA decontamination by 1N NaOH. d and d_{NaOH} indicated the proteins thicknesses before and after being treated with NaOH, respectively.

Surfaces	**Stainless steel**		**AUT**	
Thickness (nm)	**d**	**d_{NaOH}**	**d**	**d_{NaOH}**
α-Syn 10 μg/mL	1.38 ± 0.16[1]	−0.56 ± 0.01	1.92 ± 0.13	0.13 ± 0.06
α-Syn 50 μg/mL	1.30	−0.91	N/a	N/a
α-Syn 100 μg/mL	1.03	−0.66	N/a	N/a
BSA 10 μg/mL	2.18	−0.41	N/a	N/a

[1] All error bars represent ±rror bars repre

Author Manuscript Author Manuscript Author Manuscript Author Manuscript

Table 2

DLS size distribution (number %) of α-syn fibrils in Initial solution, Effluent 1, and Effluent 2 from stainless steel and AUT surfaces

Hydrodynamic diameter range (nm)	Stainless steel (Number %)			AUT (Number %)		
	Initial solution	Effluent 1	Effluent 2	Initial solution	Effluent 1	Effluent 2
0 – 2	16.7	66.7		25.0		25.0
> 2 – 5			56.0	25.0	38.0	25.0
> 5 – 10	16.7	22.0	4.0		21.0	
> 10 – 20		11.3			16.0	18.7
> 20 – 30	31.0					6.0
> 30 – 40	7.7		13.2		13.3	0.3
> 40 – 50	9.3		6.8	13.2	7.2	
> 50 – 60	1.0		13.8	9.8	2.5	
> 60 – 70	0.3		4.4	21.5	0.5	
> 70 – 80	0.5		1.8	4.3		11.0
> 80 – 90	7.0			0.5		8.3
> 90 – 100	6.0					
> 100 – 200	3.8					5.7
> 200 – 400				0.7	1.5	
Average hydrodynamic diameter	32.8 nm	3.4 nm	22.0 nm	33.7 nm	20.8 nm	26.6 nm